IOP Publishing New J. Phys. 27 (2025) 023029 https://doi.org/10.1088/1367-2630/adb510

New Journal of Physics
The open access journal at the forefront of physics

Deutsche Physikalische Gesellschaft DPG
IOP Institute of Physics

Published in partnership with: Deutsche Physikalische Gesellschaft and the Institute of Physics

OPEN ACCESS

RECEIVED
20 November 2024

REVISED
5 February 2025

ACCEPTED FOR PUBLICATION
12 February 2025

PUBLISHED
24 February 2025

PAPER

Light storage by electromagnetically induced transparency for one second at the level of a single photon in Pr^{3+}:Y_2SiO_5 prepared with multiple frequency ensembles

Marcel Hain, Niklas Stewen* and Thomas Halfmann[1]

Institut für Angewandte Physik, Technische Universität Darmstadt, Hochschulstr. 6, 64289 Darmstadt, Germany
[1] www.iap.tu-darmstadt.de/nlq.
* Author to whom any correspondence should be addressed.

E-mail: niklas.stewen@physik.tu-darmstadt.de

Keywords: quantum optics, quantum memory, EIT, single photon, rare earth doped solid

Abstract

Efficient and long-term storage of quantum information encoded in single photons is crucial for applications of optical quantum technologies, e.g. quantum repeaters in communication networks. Obviously, the maximal storage time is an important benchmark for such memories, as it defines the distances covered by the network or the applicability of quantum communication protocols therein. In this paper, we present the implementation of an optical memory driven by electromagnetically induced transparency, permitting the storage of weak coherent pulses containing on average a single photon with a signal-to-noise ratio of 1.3(3) for a long storage time of one second. To achieve this goal, we apply decoherence control by static magnetic fields and robust dynamical decoupling sequences to prolong the coherence time in a rare-earth ion doped crystal to 14 s. A novel optical preparation scheme serves to increase the optical depth of the medium, which enables a light storage efficiency of 12.7(5)% at the single photon level and one second storage time.

1. Introduction

Optical quantum memories are essential building blocks for quantum repeaters in quantum communication networks [1]. They require an efficient, high-fidelity and multiplexed storage of single photons on a sufficiently long timescale. In recent years, progress was made with regard to all these parameters. Storage efficiencies $\eta > 50\%$ [2–14], fidelities of up to 99.9% were achieved [15], the multiplexing capacity reached storage of up to 1650 modes [16–20], and a storage time of up to 100 ms was achieved [21, 22] at the single photon level. Storage times of $t_s \gtrsim 100$ ms already enable communication over distances of 1000 km between the network nodes [23, 24]. As the storage time increases, the possible entanglement rate grows [23], particularly in the low multiplexing regime, and the potential spatial dimensions of networks expand.

Important for realistic implementations, however, is an advantageous combination of all the above memory specifications. The storage efficiency is obviously important to reach entanglement rates at a reasonable level for applications. The largest reported storage efficiency at the single photon level is $\eta = 91\%$, but the decay (or storage) time of 15 μs in this gas-phase experiment was far too short to enable realistic implementations of a quantum repeater [7]. As typical features of memories in atomic gases, they offer large optical depth (OD) and therefore also high storage efficiencies, but the storage time is usually limited to (at most) the millisecond regime due to atomic motion [25, 26].

Rare-earth ion doped crystals (REICs) with their long population and coherence lifetimes (potentially up to the regime of seconds, minutes, or even hours) are an appropriate medium to implement a memory with long storage times. Light storage experiments for classical pulses in REICs yielded storage times up to 53 min in Eu^{3+}:Y_2SiO_5 and 42 s in Pr^{3+}:Y_2SiO_5 [27, 28]. However, the efficiency in these experiments was only in the regime of 0.01%–0.1%, which is an obstacle for storage at the single photon level. We previously

increased the efficiency up to 76% by application of a multi-pass setup [29]. However, the low transmission limits the end-to-end efficiency, and the increased solid angle into which noise can couple degrades the signal-to-noise ratio. This restricted the applicability for single photon storage.

There are a number of protocols to drive a memory for single photons in REICs [30]. In recent years, the atomic frequency comb (AFC) protocol probably became the most commonly applied storage protocol in such media. AFCs permit storage of time-bin qubits and the multiplexing of many temporal modes at low noise [30–34]. However, the AFC protocol requires optical preparation of spectrally narrow absorption features by a laser system with sufficiently small linewidth. Electromagnetically induced transparency (EIT) is an alternative protocol, which is also applicable at larger laser linewidth, allowing less strict requirements on the laser system [35]. Multiplexed light storage with EIT is possible by exploiting the spatial degrees of freedom [19].

In this paper, we present EIT based storage of weak coherent pulses on the single photon level for a storage time of $t_s = 1\,\mathrm{s}$, implemented in a Pr^{3+}:Y_2SiO_5 crystal (termed Pr:YSO in the rest of the paper for short). To achieve this, we push the coherence lifetime in the medium by zero first order Zeeman shifts (ZEFOZ) and robust dynamical decoupling pulse sequences to $T_2^{\mathrm{DD}} = 14\,\mathrm{s}$. To compensate for the large optical background induced by the control beam required in EIT, we apply a second Pr:YSO crystal as a spectral filter. To increase the storage efficiency, we introduce a novel preparation scheme which enables simultaneous preparation of two atomic ensembles. This increases the OD of the memory and, hence, doubles the storage efficiency to 12.7(5)%. With these measures, we achieve a signal-to-noise ratio (SNR) of 1.3(3) for storage of a single photon at a storage time of one second. We note that the preparation and filter schemes are also applicable and of benefit to other light storage protocols.

2. Two-ensemble preparation for EIT at ZEFOZ conditions

We implement EIT in a three-level system in Λ-type configuration with a probe transition at frequency ν_p and a control transition at frequency ν_c (see figure 1(e)), which depicts EIT coupling schemes in two frequency ensembles in Pr:YSO). The theory of EIT light storage is well-established, see, e.g. [35]. We therefore give only a short summary of the theory here. In EIT light storage, a strong, classical control pulse with Rabi frequency Ω_c generates a transparency window for the probe pulse, which is assumed to be weak, potentially at the single photon level. If both pulses are adiabatically switched off, the control pulse transfers the optical coherence induced by the probe field on the probe transition to a spin coherence between the two ground states in the Λ scheme. After some storage time, the spin coherence can be transferred back to a signal pulse by applying a control read pulse, i.e. the probe pulse is retrieved from the memory. The storage efficiency is determined by the available OD on the probe transition [36]. For small storage efficiencies, the efficiency grows approximately linearly with the OD.

The storage time is limited by the lifetime of the spin coherence among the ground states, which is in turn limited by the population lifetime. The latter approaches 1–2 min in Pr:YSO [28, 37]. To suppress perturbing decoherence processes and provide such long coherence time in REICs, the medium is prepared under ZEFOZ conditions [38, 39] by an appropriate static magnetic field in three dimensions. The induced Zeeman levels are less sensitive to perturbations (decoherence processes) induced by the host lattice, and hence the coherence time significantly increases. At the ZEFOZ point, the coherence time is mainly limited by limited precision, small deviations, fluctuations, or inhomogeneities in the static magnetic field for ZEFOZ, leading to non-perfect ZEFOZ conditions, i.e. the dependence of the transition frequency on the magnetic field is very small, but not fully cancelled.

In our case, we apply a field with $\vec{B}_0 = (-86, -160, 379)\,\mathrm{G}$ in a coordinate system where $x \parallel D_1$, $y \parallel D_2$, and $z \parallel b$, with the crystal axes D_1, D_2, and b.

The energy levels in REICs are typically split into hyperfine manifolds, and optical transitions in the dopant ions are strongly inhomogeneously broadened. In Pr:YSO, the transitions in the $^3H_4 \leftrightarrow {}^1D_2$ manifold around the center wavelength of 606 nm have a homogeneous width of a few kHz, with frequency differences between the hyperfine states on the order of 10 MHz, and an inhomogeneous optical linewidth of some GHz. Hence, a single laser field will drive different optical transitions in different dopand ions of the broad inhomogenous manifold simultaneously. Thus, we need to prepare the atomic populations in the hyperfine ground states via optical pumping to obtain a proper three-level system as required by EIT.

We classify all ions in which the same transition is coupled to the same laser frequency as a frequency ensemble. At magnetic field $\vec{B}_0$ in Pr:YSO, we get six Zeeman ground states $|0\rangle_g$ to $|5\rangle_g$ and six optically excited states $|0\rangle_e$ to $|5\rangle_e$ in each of the two magnetic sites, i.e. 36 optical transitions per site. Figure 1(a) shows the level scheme in the magnetic site that we use for our experiments. The ZEFOZ condition occurs between states $|3\rangle_g$ and $|5\rangle_g$ (highlighted in green in figure 1(a)). A common technique to permit experiments on isolated transitions in a well-defined frequency ensemble is to optically pump the population

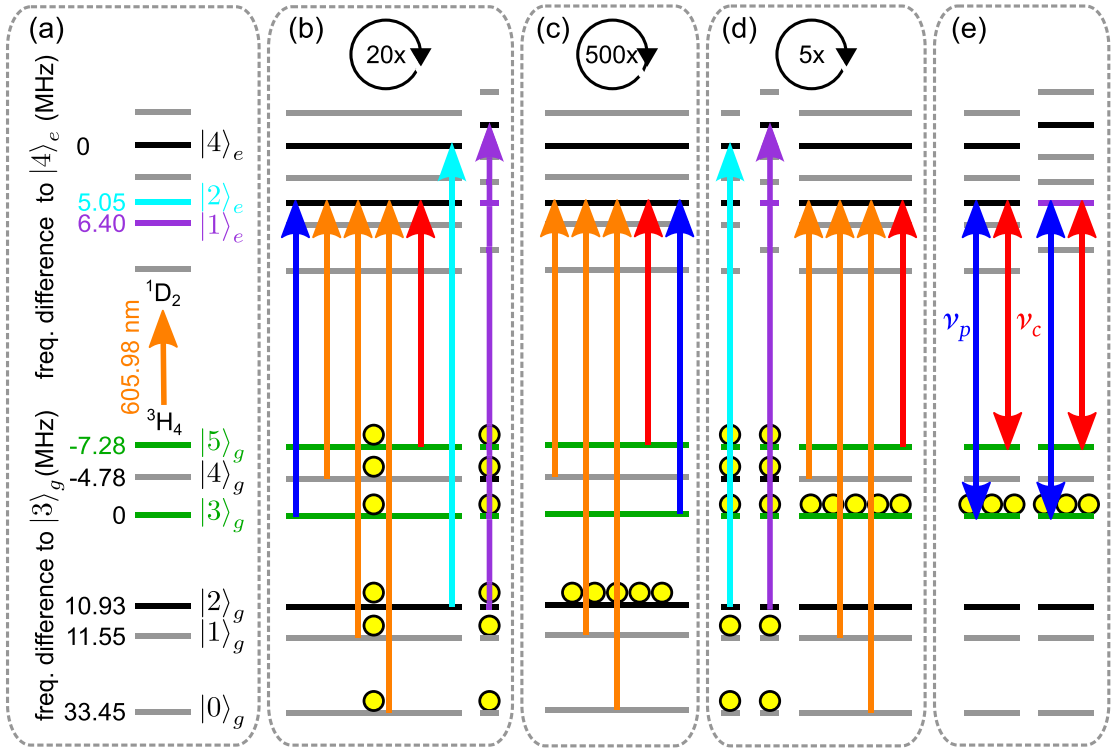

Figure 1. Two-ensemble preparation scheme for EIT light storage in Pr:YSO under ZEFOZ conditions. (a) Level scheme of Pr:YSO with Zeeman splittings. The relevant hyperfine ground states at ZEFOZ are highlighted in green. The excited states used for EIT in the first and second ensemble are shown in cyan and purple. The center of the optical transition is at 605.98 nm. The energetic positions of the Zeeman-split hyperfine levels are given relative to levels $|3\rangle_g$ or $|4\rangle_e$. (b)–(d) Preparation steps: class cleaning, spin polarization, and backburning & cleaning. We indicate the transitions coupled by the laser pulses in the target ensembles of the preparation as arrows. In order not to overload the plot, we do not indicate chirps on the laser frequencies. We depict pulses, which only couple (resonantly) to ϵ_1 in cyan, and pulses which couple only to ϵ_2 in purple. Red and blue arrows indicate the control and probe transition. Yellow disks represent the population of the ground state after each preparation step. Numbers above the level schemes give the typical number of repetitions of the preparation steps. (e) EIT coupling schemes in the two optically prepared frequency ensembles.

in undesired ensembles to other ground states and 'shelve' it therein [40, 41]. In order to achieve this shelving despite the simultaneous coupling of 72 transitions, we apply a scheme based on spectral hole burning first described by Lauritzen *et al* [42]. This prepares an isolated absorption peak as part of a Λ-type level scheme for EIT. We develop an extension of this scheme to simultaneously prepare two ensembles, which results in an increased OD and higher storage efficiency. In the following, we describe this preparation scheme.

In the first step of the preparation, called 'class cleaning' because it removes absorption in undesired ensembles at the relevant frequencies, we address the populations in all six ground states by using a series of laser pulses to drive the populations into an excited state (see figure 1(b)). The population then immediately decays back to the ground states. We chirp the pulses over a frequency range $\Delta\nu$ in order to suppress off-resonant couplings in later steps. In the target ensemble, the pulses couple five of the six ground state (all except $|2\rangle_g$) to the same excited state ($|2\rangle_e$ for the first ensemble ϵ_1, blue, orange, and red arrows in figure 1(b)), while we couple $|2\rangle_g$ to $|4\rangle_e$ (cyan arrow in figure 1(b)). Thus, the population in the target ensemble is shuffled between all ground states. However, the main impact of the class cleaning step is not on the target ensemble but on other ensembles in which the pulses also pump population, but couple to different ground states and/or to different excited states. In these undesired ensembles, at least one ground state remains uncoupled and collects the atomic population. Thus, after class cleaning, pulses with any of the laser frequencies used so far will only couple the populations in the target ensemble. In order to add a second target ensemble ϵ_2, we simply add a chirped pulse to the end of each class cleaning cycle (see the purple arrow in figure 1(b)). This pulse couples the transition $|2\rangle_g \leftrightarrow |4\rangle_e$ in ensemble ϵ_2. If the frequency shift between the ensembles is chosen such that the first five pulses also couple to an excited state in ϵ_2 (state $|1\rangle_e$ in our case), then the population is prepared in both ensembles simultaneously.

In the second step, called 'spin polarization', we repeat the first five chirped laser pulses from the class cleaning step, but in a different order (see the orange, red, and blue arrows in figure 1(c)). The population thereby accumulates in state $|2\rangle_g$, and the spin state of the nucleus is 'polarized' to state $|2\rangle_g$ (see the yellow disks in figure 1(c)). To conclude the second step, we apply a pulse with a chirp around ν_p (see the blue arrow

in figure 1(c)) to ensure full transparency. This enables a probe pulse reference measurement after this step for later calibration of the storage efficiency.

As a third step, called 'backburning & cleaning' (see figure 1(d)), we apply two fixed frequency backburning pulses (see the cyan and purple arrows in figure 1(d)) to redistribute the population in ϵ_1 and ϵ_2 from $|2\rangle_g$ to $|3\rangle_g$. Since part of the population decays into the other ground states, we then clean it by applying chirped pulses to the remaining four states (see the orange and red arrows in figure 1(d)). Now, we have prepared a background-free absorption peak in the center of the previously prepared transmission window, which stems only from the $|3\rangle_g \leftrightarrow |2\rangle_e$ transition in ϵ_1 and $|3\rangle_g \leftrightarrow |1\rangle_e$ in ϵ_2. Furthermore, there is almost no absorption in a spectral range of width $\Delta\nu$ around the EIT control frequency ν_c, which enables us to apply the control pulse for EIT light storage (see figure 1(e)). To ensure perfect transmission at ν_c even for imperfect pumping, we apply the pulse around ν_c at the end of the sequence (see the red arrow in figure 1(d)). We note that backburning via $|3\rangle_e$ instead of $|4\rangle_e$ is also possible, but resulted in a small background absorption of OD ~ 0.1 in our experiments. Although this could possibly be avoided by further optimization of the preparation parameters, we apply the backburning pulses on the $|2\rangle_g \leftrightarrow |4\rangle_e$ transition.

We note that in our light storage experiments, we also apply dynamical decoupling of the spin coherence by radio-frequency (RF) rephasing pulses on the magnetic dipole transition $|3\rangle_g \leftrightarrow |5\rangle_g$. Since RF pulse errors cause a partial population transfer in all ensembles, we will get some undesired absorption at the control and probe frequency after each rephasing sequence. Absorption of control pulses at ν_c causes noise by fluorescence and Raman scattering, while absorption of retrieved signal pulses at ν_p reduces the storage efficiency. To avoid these effects, we slightly modify the preparation sequence described above and add two chirped pulses before each class cleaning cycle (not depicted in figure 1). These pulses are centered at $\nu_c - \nu_{RF}$ and $\nu_p + \nu_{RF}$, where ν_{RF} is the frequency of the transition $|3\rangle_g \leftrightarrow |5\rangle_g$. This creates additional spectral pits such that no population can be driven by the RF rephasing pulses in the ensembles ϵ_1 and ϵ_2. The spectral pits are not fully preserved after the remainder of the preparation sequence, but in the two ensembles $\epsilon_{1,2} \pm \nu_{RF}$, the states $|3\rangle_g$ and $|5\rangle_g$ which contain the spin coherence remain unpopulated.

To implement the preparation scheme as described above, we require the optimal pulse parameters for the extended pumping sequences, i.e. pulse intensities, duration, chirp range, repetition rate of the preparation steps, etc. From a numerical simulation of the optical pumping processes, we determine start parameters, which are refined by an experimental optimization afterward. The parameters obtained may vary due to changes in the setup and the environment. The goal is to obtain a narrow absorption peak with large OD and vanishing background absorption, which we monitor by time-resolved absorption spectroscopy during the preparation sequence. In total, the preparation sequence takes roughly one second, and we repeat it prior to every single EIT light storage measurement to maintain optimal conditions.

In principle, the concept of simultaneous optical preparation can be extended to more than two frequency ensembles. In practice, however, the many required additional preparation pulses can interact and perturb the population distribution in the targeted ensembles. Thus, the maximal number of ensembles will depend upon the specific medium and excitation scheme.

3. Experimental setup

Figure 2 schematically depicts the experimental setup. The Pr:YSO sample (Scientific Materials) with a dopant level of 0.02% and dimensions 5 mm × 5 mm × 3 mm (along the D_1, D_2, and b-axes) is mounted in a continuous-flow cryostat (ST-100, Janis) for cooling below 4 K. We apply three pairs of superconducting Helmholtz coils to provide the field $\vec{B}_0$ for ZEFOZ, and an additional pair of Helmholtz coils to provide RF rephasing pulses. Before each measurement, we optimize $\vec{B}_0$ via a gradient descent algorithm to compensate for daily fluctuations in the magnetic background field and other drifts induced by the environment.

Our laser source (DLC TA-SHG pro 24509, Toptica) is an external-cavity diode laser (ECDL) operating at a wavelength of 1212 nm, equipped with a tapered amplifier and a cavity-enhanced second harmonic generation stage. This provides the radiation at 606 nm to drive the optical transition $^3H_4 \leftrightarrow {}^1D_2$ in Pr:YSO. The laser system is frequency stabilized to a linewidth of roughly 20 kHz by using a home-made Pound–Drever–Hall unit involving a reference cavity.

We split the laser beam into a strong control/preparation beam line and a weak probe beam line. We use acousto-optic modulators in double-pass configuration for frequency and amplitude modulation in the beam lines. For storage of weak coherent pulses, we attenuate the probe beam by using neutral density filters. Both beams are polarized along the D_2 axis of the Pr:YSO sample and counter-propagating along the b-axis with a small angle of $\sim 1°$. In the sample, the beam diameters (beam waist $2w_0$) are 365 μm (control) and 180 μm (probe). We found that a proper choice of sufficiently small diameter for the control beam significantly reduced the level of optical noise—probably due to the smaller interaction volume in the crystal in which noise photons are generated by the control pulse. Therefore, we reduced the diameter of the laser

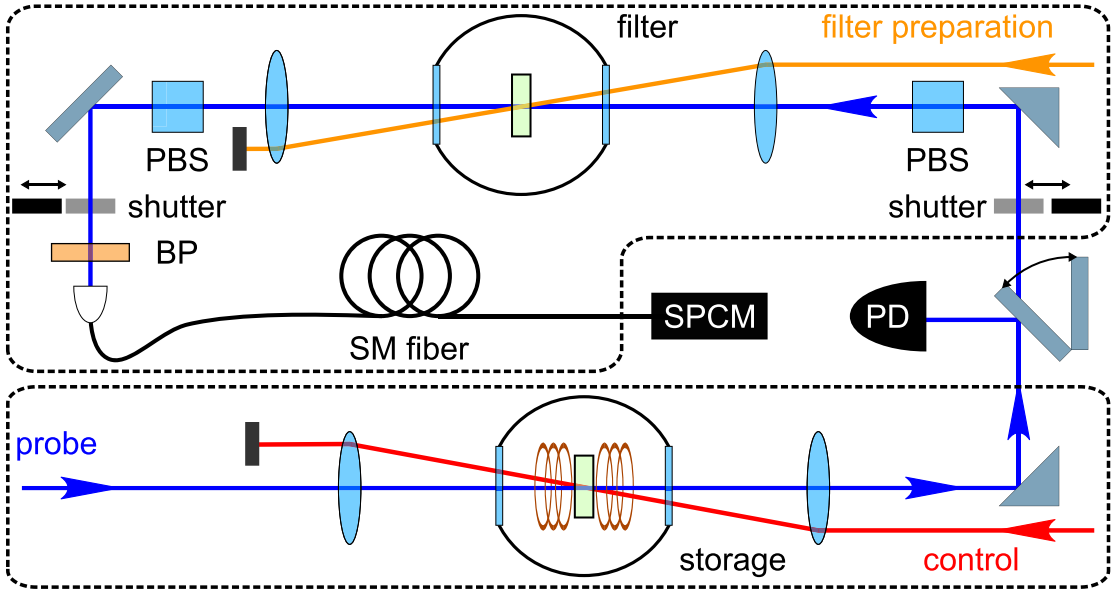

Figure 2. Experimental setup. The lower box shows the storage setup, the upper box the filter setup. The blue, red, and orange lines represent probe, control, and filter preparation beam lines. The cryostats host the crystals (light green) and several coil pairs for static and RF magnetic fields. Other relevant items in the optical setup are photo diode (PD), single photon counting module (SPCM), band pass filter (BP), polarizing beam splitter (PBS), and single mode (SM) optical fiber.

beams in comparison to our previous work on EIT light storage [43]. We also optimized the intensity of the preparation pulses for a low noise level, as incomplete optical pumping (at too low power) or spectral broadening (at too high power) may lead to noise by Raman scattering in off-resonant ensembles. For storage of classical probe pulses, we detect the signal using a photodiode (New Focus 2051-FS). For storage of weak coherent pulses, the probe beam passes a spectral filter to suppress the large optical background generated by the control beam—which temporally fully overlaps with the retrieved weak signal pulse in EIT. Thus, suppression of the large noise generated by the strong classical control field with frequency very close to the probe/signal pulse is crucial to permit observation of a signal at the single photon level. After the spectral filter, we couple the probe/signal beam into a single mode fiber and use a single photon counting module (SPCM, Excelitas Technologies SPCM-AQRH-43-FC) for detection.

The spectral filter is based on a second Pr:YSO crystal (Scientific Materials, $5 \times 5 \times 3$ mm, dopant level 1%) in a cryostat. We optically pump the filter crystal to provide a 600 kHz narrow transmission window centered at ν_p, which blocks scattered radiation from the control beam but transmits the signal beam. We added a dielectric band pass filter to further enhance suppression of broader-band optical noise. Compared to previous work [43], we now apply a band pass filter with a narrower transmission window of 0.34 nm (FWHM) (Laser Components), and added a polarizing beam splitter cube (PBS) as well as a shutter between the storage and filter cryostats. The PBS helps to filter unpolarized noise. The shutter blocks stray light emitted during the optical preparation steps of the storage or filter crystal from reaching the other crystal. Otherwise, the filter preparation sequence could reduce the OD of the storage crystal at ν_p and the cleaning pulses at ν_c could reduce the filter absorption. The spectral filter permits in total a background suppression of up to ∼60 dB at ν_c in a single pass. This results in a larger suppression (roughly by a factor of ∼10 dB) compared to our previous work even though there we used the filter crystal in a double pass configuration. This improved performance is also due to a lower broadband background of our ECDL-based system, which replaced the system based on an optical parameteric oscillator (OPO) used in our previous experiments on EIT light storage. The large acceptance bandwidth of an OPO in the range of several 100 GHz (corresponding to some 0.1 nm in the visible regime) typically produces a spectrally broad pedestal of optical noise—which is not the case in an ECDL. This broad pedestal from the OPO is very weak, but becomes relevant at the low light level of single photon storage. Finally, by arranging the probe and control beam in counter-propagating geometry and spatial filtering of the signal beam by the single mode fiber to the SPCM, we reach a total suppression of the control field by ∼90 dB. This is crucial to permit the observation of single photon storage by EIT. The total transmission of the probe beam (measured from the entrance window of the storage cryostat to the SPCM) is 18%, yielding a total detection efficiency of 12% after taking the detector efficiency into account. We note that we could, in principle, even further increase the filter performance by applying the filter crystal in multi-pass. However, the double pass would also reduce transmission at the signal/probe

frequency, and hence increase the time required for systematic measurements, which at storage times up to one second was already very long. As the filter performance in single pass with a suppression of ∼90 dB at the control frequency was fully sufficient for single photon storage, we decided to proceed with this simpler setup.

4. Experimental results

We start our measurements by optimizing the parameters of the preparation sequence in order to obtain maximal OD at the probe transition frequency ν_p. To do so, we first individually prepare and optimize the absorption for each of the two ensembles. The measured absorption spectra are shown in figure 3(a). We measured the absorption spectra using a chirped probe pulse which we attenuate to the few-photon level ($\sim$1 photon μs^{-1}) using neutral density filters. The chirp must be kept sufficiently slow to avoid distortions of the spectra [44]. The absorption lines have a spectral width of ∼45 kHz (FWHM), which is determined by the inhomogeneous linewidth of the $|2\rangle_g \leftrightarrow |3\rangle_g$ transition (approx. 10 kHz), the laser linewidth (approx. 20 kHz), and additional broadening effects, e.g. instantaneous spectral diffusion and power broadening.

The peak ODs for the two ensembles are OD = 3.2 and 2.3 as determined via Lorentzian fits. The ODs are different because the transition moments in the two ensembles are different, and the population in the ground states $|3\rangle_g$ might also differ due to imperfect optical pumping. We could further slightly improve the OD by 7% and 3% respectively, by increasing the power of the backburning pulses, but this also increased the spectral linewidths by 46% and 24%, indicating the onset of undesired broadening mechanisms. We note that in previous work [43], we implemented EIT light storage in a medium with lower optical depth and, hence, lower storage efficiency. Our improved preparation scheme now enables considerably larger OD and storage efficiency (see green diamonds in figure 3(a)). The peak OD is OD = 4.7 and the spectral linewidth is 45 kHz (FWHM). The OD is slightly lower than the sum of the OD of the two individually prepared ensembles, which indicates some perturbing crosstalk during the two preparation sequences. Nevertheless, the improvement in OD is a factor of 2 compared to the single-ensemble preparation in our previous work [43].

The efficiency of the EIT light storage protocol also depends upon the control Rabi frequency Ω_c. It must be matched to the duration of the probe pulse, i.e. Ω_c must be sufficiently large to provide a transparency window which covers the probe pulse spectrum, but also sufficiently small to provide a steep dispersion and compression of the probe pulse in the medium [35]. For EIT light storage in two ensembles, we must fulfill this conditions in each of them, i.e. Ω_c should be similar in both ensembles. This would also be advantageous for simultaneous application of other storage protocols (e.g. AFC spin storage) in different ensembles. Figure 3(b) shows the absorption spectra under EIT conditions in the two ensembles for two different control powers P_c. We find that for both low $P_c = 60\,\mu$W and high $P_c = 20$ mW, the splitting of the absorption peak is essentially the same in both ensembles. This indicates identical transition dipole moments at the control transitions, i.e. equal Rabi frequencies, which happens to be the optimal case for simultaneous light storage in the two ensembles (regardless of whether by EIT or other protocols, such as AFC). However, the basic concept of the two-ensemble preparation also works for ensembles with different transition moments, provided robust mapping pulses are applied to cover the difference.

We note that for quite high control powers, we observe some Raman absorption within the EIT window, yielding a small peak with OD ≈ 0.2 at a control power of $P_c = 20$ mW. Since we perform the light storage experiments at moderate powers up to $P_c = 2$ mW, Raman absorption only plays a minor role. It stems from ensembles which absorb at the edges of the spectral pit of the probe transition, i.e. with a single photon detuning of at least 200 kHz. At a first glance, it might seem that Raman absorption in the EIT window reduces the storage efficiency due to absorption of the probe and signal pulses. However, Raman-type light storage (which can be understood as an off-resonant EIT protocol) indeed increases the storage efficiency [45]. Although simultaneous storage via EIT in the resonant ensembles and via Raman absorption in the off-resonant ensembles could be used to further increase the storage efficiency, we tried to avoid Raman absorption by appropriate design of the preparation sequence in order to investigate proper EIT conditions in our memory. Nevertheless, we always determined the small amount of Raman absorption in our measurements by skipping the backburning pulses in the preparation sequence, i.e. by not preparing the absorption peak at ν_p, and recording a spectrum. We subtracted it from the EIT spectra to obtain the data shown in figure 3(b).

For further analysis, we fit the EIT spectrum [35] (solid lines in figure 3(b)) and get the control Rabi frequency Ω_c. Figure 3(c) shows the obtained variation of the control Rabi frequency Ω_c with the control power P_c for the two ensembles, as well as for simultaneous preparation of both ensembles. Over a variation of P_c in three orders of magnitude, there is no difference between the values for Ω_c in the two single ensembles or for their simultaneous preparations. We fit a power law $\Omega_c = a \cdot (P_c)^b$ to the data, since we expect $\Omega_c \propto \sqrt{P_c}$, i.e. an exponent of 0.5. The dashed lines in figure 3(c) show the fit results, which confirm

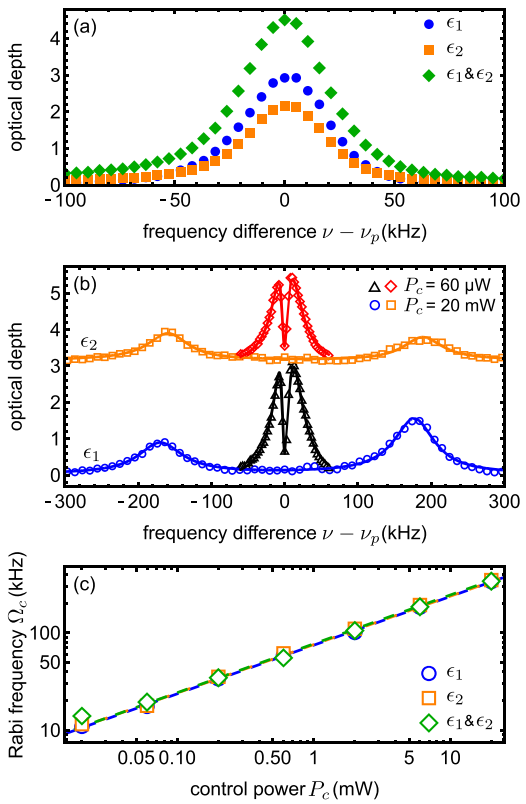

Figure 3. (a) Absorption spectra after preparation of two individual frequency ensembles (blue disks and orange squares for ϵ_1 and ϵ_2) and after simultaneous preparation of both ensembles (green diamonds). (b) Absorption spectra at EIT conditions in ϵ_1 (blue circles and black triangles) and in ϵ_2 (orange squares and red diamonds, shifted up by OD = 3 for clarity) for control power $P_c = 20\,\mathrm{mW}$ (blue circles and orange squares) or $P_c = 60\,\mu\mathrm{W}$ (black triangles and red diamonds). Symbols represent experimental data, solid lines are fit functions according to [35]. (c) Dependence of the Rabi frequency Ω_c vs P_c determined from the EIT spectra, for the individual ensembles and after simultaneous preparation of both ensembles. Note the logarithmic scales on both axes. Dashed lines show power functions $\Omega_c = a \cdot (P_c)^b$ with a and b as fit parameters.

the exponent $b = 0.500(3)$ and yield a proportionality constant $a = 2\pi \times 76.1(4)\,\mathrm{kHz}\sqrt{\mathrm{mW}}^{-1}$. The control Rabi frequency values for ϵ_1 and ϵ_2 are the same within the precision of our measurement. From this result, we estimate $\mu \approx 3 \times 10^{-33}\,\mathrm{C\,m}$ on the $|5\rangle_g \leftrightarrow |1\rangle_e$ and $|5\rangle_g \leftrightarrow |2\rangle_e$ transitions, which roughly agrees with the values in the range of 1.2×10^{-32} to $3.7 \times 10^{-32}\,\mathrm{C\,m}$ previously reported for Pr:YSO [41, 46, 47].

We now proceed to EIT light storage of classical probe pulses with a power of $P_\mathrm{p} = 100\,\mu\mathrm{W}$, first at a short storage time of $2\,\mu\mathrm{s}$, without rephasing by RF pulses. We set the control power of the rectangular control pulses to $P_\mathrm{c} = 2\,\mathrm{mW}$ (corresponding to a Rabi frequency of $\Omega_\mathrm{c} = 2\pi \times 110\,\mathrm{kHz}$), which matches with probe pulses with a duration of $7.5\,\mu\mathrm{s}$. As the storage efficiency depends upon the temporal shape of the probe pulse, we follow the procedure described in [48, 49] to iteratively optimize the pulse shape towards maximal storage efficiency. We obtain an efficiency of $\eta_0 = 15.5(5)\%$ at the short storage time of $2\,\mu\mathrm{s}$, which is far below the dephasing time of $T_2^* = 1/\Gamma_\mathrm{inh} \approx 200\,\mu\mathrm{s}$ due to the inhomogeneous broadening Γ_inh of the spin transition $|3\rangle_g \leftrightarrow |5\rangle_g$. Therefore, rephasing was not required in this measurement. From theory, we expect a storage efficiency of $\sim$25% for an OD of $\sim$4.7 [36]. However, the latter theory is valid for zero magnetic field only. This may already explain a deviation from the observed value of $\sim$15.5(5)% for the maximal storage efficiency in our experiment. Moreover, we suspect residual background absorption and interference of EIT with residual off-resonant Raman-type interactions to further reduce the efficiency.

For EIT light storage towards longer storage times, we now apply ZEFOZ and simple 'spin-echo' rephasing by two RF π-pulses of duration $35\,\mu\mathrm{s}$. We measure the light storage efficiency vs the storage time. Figure 4(a) shows the results for classical pulses. A Gaussian fit, which is in accord with the theory given in [50], yields a $1/e$ decay time of $T_2^\mathrm{SE} = 1.83(4)\,\mathrm{s}$. Thus, the decoherence control by ZEFOZ and rephasing permits the prolongation of the storage (or coherence) time by almost four orders of magnitude compared to T_2^*. From the storage efficiency of $\eta_\mathrm{SE} = 9.8(2)\%$ at $t_\mathrm{s} = 200\,\mathrm{ms}$, we estimate the rephasing efficiency of the π-pulses as $\eta_\pi = \sqrt{\eta_\mathrm{SE}/\eta_0} \approx 80\%$. Here, we assume pulse errors to be the only deteriorating effect at this storage time t_s, since $t_\mathrm{s} \ll T_2^\mathrm{SE}$. We note that we improved η_π by a factor of 2 compared to our previous work [43]. We further prolong t_s by applying dynamical decoupling, i.e. a sequence of π-pulses in which the time separation is ideally shorter than the typical timescale of decoherence processes induced by the environment

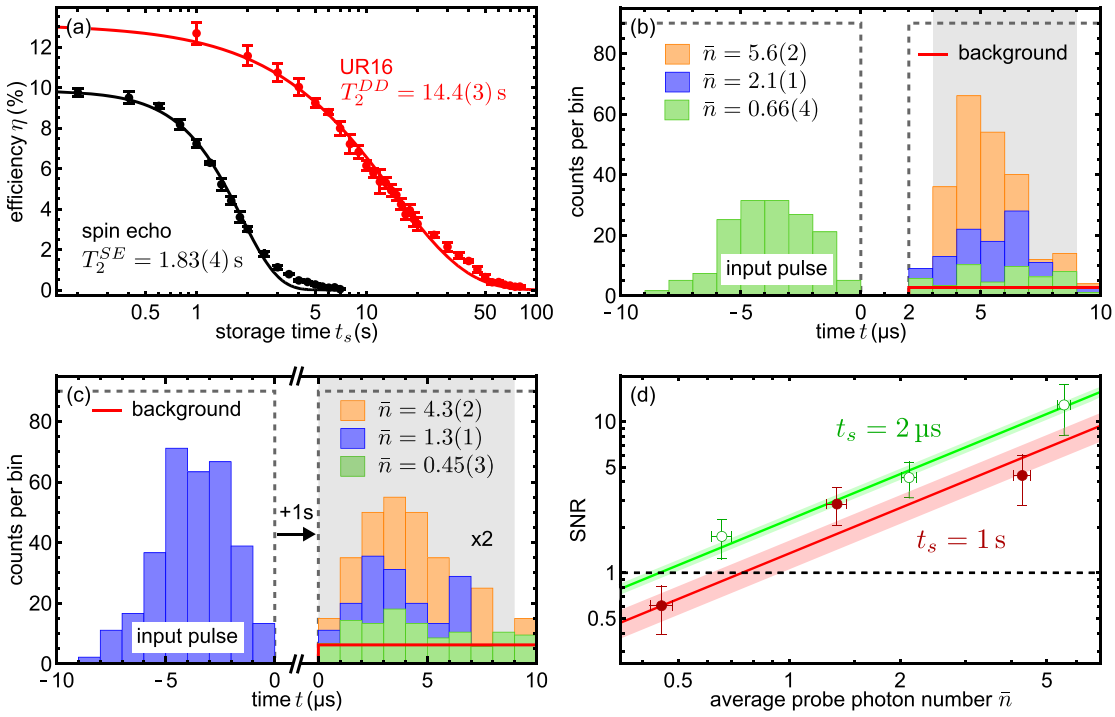

Figure 4. (a) EIT light storage efficiency η vs storage time t_s (experimental data) for classical pulses and rephasing by two simple π-pulses (black data points) or a universally robust UR16 composite sequence (red data points) under ZEFOZ conditions. The black and red lines represent a Gaussian and an exponential fit. Note the logarithmic scale on the time axis. (b) Histogram of photon counts for EIT light storage of weak coherent pulses under ZEFOZ conditions, but without rephasing pulses. The storage time was $t_s = 2\,\mu$s. Orange, blue and green bars show the counts for different mean number of probe photons $\bar{n}$. We only show the probe pulse for $\bar{n} = 0.66(4)$. The data were collected in 1000, 2000, and 3500 experimental runs for $\bar{n} = 5.6(2)$, $\bar{n} = 2.1(1)$, and $\bar{n} = 0.66(4)$, and scaled to 2000 runs to permit appearance in the same plot. The gray dashed line represents the timing of the control pulses, and the red solid line indicates the averaged noise level during the signal integration time (gray shaded area). (c) Photon counting histogram for storage of weak coherent pulses at the single photon level for a long storage time of $t_s = 1$ s. Note that in this plot, we magnify the signal pulses and average noise level by a factor of 2 and interrupt the time axis between storage and retrieval. We collected the data in 800, 1800, and 4200 runs for $\bar{n} = 4.3(2)$, $\bar{n} = 1.3(1)$, and $\bar{n} = 0.45(3)$, and scaled all data to 2000 runs. (d) Variation of the SNR vs mean photon number $\bar{n}$ for storage times of $t_s = 2\,\mu$s (green) and $t_s = 1$ s (red) corresponding to the data shown in (b) and (c). The solid lines and shaded areas indicate linear fits with uncertainty regions. The dashed line marks the threshold SNR = 1. Note the logarithmic scale on the SNR axis.

medium [51]. However, we cannot decrease the pulse separation below ~50 ms (or increase the number of pulses per time interval accordingly) because of heating of the cryogenically cooled crystal by the large number of RF pulses. Thus, the time separation of the π-pulses is much longer than the typical timescale of decoherence processes induced by the environment medium, and it is not dynamical decoupling in the strict sense. Nevertheless, as will be shown below, the technique still improves the coherence time by roughly an order of magnitude.

To compensate for pulse errors, we apply a robust composite pulse sequence. The UR16 sequence [52] with a total duration of 1 s and pulse separation 62.5 ms very efficiently compensates for the amplitude and detuning errors of the RF pulses. Since the UR16 sequence is most robust for a pulse area slightly smaller than π, we apply pulses with a duration of 32.5 μs, i.e. slightly shorter than π-pulses, to achieve maximal rephasing efficiency. We vary the storage time t_s by increasing the number of cycles of the UR16 sequence without changing the pulse separation. Figure 4(a) shows the measured variation of the light storage efficiency η with t_s. For $t_s = 1$ s, i.e. a single UR16 sequence, we get $\eta = 12.7(5)\%$. This is only 3% lower than the efficiency without any rephasing—despite the application of 16 π-pulses and the increase in storage time by six orders of magnitude. In a conventional CPMG [53, 54] sequence of 16 identical π-pulses, we would get an efficiency of the rephasing sequence of $(\eta_\pi)^{16} = 0.8^{16} = 2.8\%$ only, compared to a rephasing efficiency of $\eta_{UR} = 82(4)\%$ in our UR16 sequence. The composite sequence UR16 obviously compensates very well for arbitrary pulse errors and outperforms conventional sequences. An exponential fit, as predicted by theory in [50], to the data in figure 4(a) yields a decay time of $T_2^{DD} = 14.4(3)$ s, permitting EIT storage of classical light pulses in the regime well above 10 s and with an efficiency well above 10%. Note that the coherence time is shorter than our record of 42 s for EIT storage of classical pulses in Pr:YSO [28]. The latter work used CPMG sequences for dynamical decoupling, which preserves the coherence of only a small subset of phases very

well [55]. The UR16 sequences used in our present experiment for single photon storage are applicable for arbitrary phase and thus permits a much larger storage efficiency.

We proceed to apply our setup to storage of weak coherent pulses, i.e. to pulses at or near the single photon level. First, we characterize our setup at a short storage time of $t_s = 2\,\mu$s at ZEFOZ conditions, but without RF rephasing pulses. Figure 4(b) shows the photon counting histogram (i.e. the number of probe photons and retrieved signal photons vs time, detected at the SPCM) for storage of weak coherent pulses with different mean number of probe photons $\bar{n}$. Obviously, the memory is applicable at the level of very few or single photons, i.e. the retrieved signal pulses for $\bar{n} = 2.1(1)$ and $5.6(2)$ are very clearly detectable well above the background noise level (see red line in the graph). Even for the lowest number of probe photons, $\bar{n} = 0.66(4)$, the retrieved signal is clearly visible above the background noise level of $8(1) \times 10^{-3}$ counts per shot. The average few-photon storage efficiency of $\eta_0' = 16(1)\%$ is consistent with $\eta_0 = 15.5(5)\%$, which we measured for storage of classical pulses (see above).

We add now a single UR16 rephasing sequence to enable storage of weak coherent pulses for one second. Figure 4(c) shows the measured photon counting histogram. As it was to be expected, the noise level at this long storage time increases to $14(1) \times 10^{-3}$ counts per shot, which is a factor of 2 larger than for the short storage time of $t_s = 2\,\mu$s. We attribute this to remaining imperfections of the rephasing sequence despite its robustness [56]. Nevertheless, even at this very long storage time of one second, the retrieved signal pulses at the few-photon level of $\bar{n} = 4.3(1)$, close to the single photon level $\bar{n} = 1.3(1)$, or even down to $\bar{n} = 0.45(3)$ are detectable above the background. In the latter case of $\bar{n} = 0.45(3)$, we determine SNR $= 0.6(2)$. The average storage efficiency in these measurements at the single photon level is $\eta' = 13(2)\%$, which is consistent with the value of $\eta = 12.7(5)\%$ for classical pulses.

In figure 4(d), we plot the SNR vs the mean number of probe photons $\bar{n}$ and a linear fit for the two measurement series at short and long storage times, according to figures 4(b) and (c). From the fit for short storage time $t_s = 2\,\mu$s, we see that for storage of a single photon, $\bar{n} \approx 1$, we obtain SNR $= 2.2(2)$. From the fit for long storage time $t_s = 1$ s, we find that for single photon storage we still maintain an SNR of $1.3(3)$. If we define a detection threshold by the typical condition SNR $= 1$, we see that this is reached at a probe level of $0.7(2)$ photons. Thus, the retrieved signal at the level of a single probe photon is well above the background noise even at this very long storage time. This confirms the conclusion we had already drawn earlier based on the data in figure 4(c): The EIT-driven memory in the Pr:YSO crystal is applicable for storage of single photons, permitting a long storage time of one second and efficiency over 10%. This serves as an important step towards the potential implementation as a quantum memory.

We note that we could even further improve the SNR in our setup by investigating alternative rephasing sequences and optimizing them towards low noise level. Even if their efficiency is a bit lower than the UR16 sequence, the SNR could improve [56]. However, it is very time-consuming to run such an optimizing procedure on the long timescale of one second and already low noise level at which we measure a noise photon only after many trials. Thus, we left this option for future investigations. Also, we must not fail to mention that both ZEFOZ, as demonstrated in our previous work [43], and dynamical decoupling, as shown here, increase the noise and thus, decrease the SNR of our memory, which is a price to pay for prolongation of the storage time by six orders of magnitude in our experiment.

To the best of our knowledge, our experiment is the first demonstration of single photon storage at a long timescale of one second. Previous implementations of single photon storage by EIT applied in cold atomic gases and were limited to storage times in the millisecond regime due to atomic motion and magnetic field inhomogeneity [57]. A storage time of 100 ms was achieved in a single trapped Rubidium atom at an efficiency of 22% using an off-resonant Raman storage protocol and an optical cavity to enhance the OD [21]. As a particular benefit over gases, solid state systems (or the emitters and memories implemented therein) do not suffer from atomic motion. They are already 'trapped' in space, which is a significant advantage. In Eu:YSO, storage of weak coherent pulses at the single photon level for as long as 100 ms with $2.60(2)\%$ efficiency was implemented using the AFC protocol [22]. Our memory exceeds this storage time by one order of magnitude and the efficiency by a factor of 5. We note that AFC requires a laser at smaller linewidth compared to EIT, but on the other hand permits lower background level (as the retrieved signal pulse is delayed with respect to the control readout pulse) and facilitates temporal multimode storage. Therefore in future investigations, we plan to apply our setup for single photon storage by AFC towards very long storage times as well.

5. Summary and conclusion

We experimentally demonstrated an optical EIT-driven memory in a Pr:YSO crystal capable of storing a single photon for a very long timescale of one second, at a storage efficiency of $12.7(5)\%$. If we define the detection limit by a signal-to-noise-ratio SNR $= 1$, this permits a threshold as low as $0.7(2)$ photons stored

in our memory. Thus, the retrieved signal at the level of a single probe photon is well above the background noise even at the very long storage time of one second. To achieve these results, we prolonged the coherence time in the medium by ZEFOZ [38, 39] and rephasing with universally robust UR16 [52] composite pulse sequences to 14 s. Compared to our previous work on EIT light storage [43], we modified our optical setup to reduce the noise level by a factor of ∼5. This was possible by several technical improvements in the setup of a spectral filter. Moreover, we developed and applied an optimized optical preparation, which permitted EIT light storage in two frequency ensembles in the doped solid simultaneously. The latter measure doubled the OD to 4.7 and as well pushed the storage efficiency of the memory by a factor of 2. The concepts are also applicable to alternative light storage protocols and other REICs.

Data availability statement

The data that support the findings of this study are available upon reasonable request from the authors.

Acknowledgments

The authors thank T Güntzel for experimental support in the development of the preparation sequence. We acknowledge financial support by the Federal Ministry of Education and Research (BMBF), Project No. 16KISQ030.

ORCID iDs

Marcel Hain https://orcid.org/0000-0001-8213-0797
Niklas Stewen https://orcid.org/0009-0002-8584-1943
Thomas Halfmann https://orcid.org/0000-0002-1222-2669

References

[1] Briegel H-J, Dür W, Cirac J I and Zoller P 1998 *Phys. Rev. Lett.* **81** 5932
[2] Hedges M P, Longdell J J, Li Y and Sellars M J 2010 *Nature* **465** 1052
[3] Hosseini M, Campbell G, Sparkes B M, Lam P K and Buchler B C 2011 *Nat. Phys.* **7** 794
[4] Lettner M, Mücke M, Riedl S, Vo C, Hahn C, Baur S, Bochmann J, Ritter S, Dürr S and Rempe G 2011 *Phys. Rev. Lett.* **106** 210503
[5] Cho Y-W, Campbell G T, Everett J L, Bernu J, Higginbottom D B, Cao M T, Geng J, Robins N P, Lam P K and Buchler B C 2016 *Optica* **3** 100
[6] Vernaz-Gris P, Huang K, Cao M, Sheremet A S and Laurat J 2018 *Nat. Commun.* **9** 363
[7] Wang Y, Li J, Zhang S, Su K, Zhou Y, Liao K, Du S, Yan H and Zhu S-L 2019 *Nat. Photon.* **13** 346
[8] Guo J, Feng X, Yang P, Yu Z, Chen L Q, Yuan C-H and Zhang W 2019 *Nat. Commun.* **10** 148
[9] Cao M, Hoffet F, Qiu S, Sheremet A S and Laurat J 2020 *Optica* **7** 1440
[10] Ma L, Lei X, Yan J, Li R, Chai T, Yan Z, Jia X, Xie C and Peng K 2022 *Nat. Commun.* **13** 2368
[11] Dong M-X, Zhang W-H, Zeng L, Ye Y-H, Li D-C, Guo G-C, Ding D-S and Shi B-S 2023 *Phys. Rev. Lett.* **131** 240801
[12] Davidson O, Yogev O, Poem E and Firstenberg O 2023 *Commun. Phys.* **6** 131
[13] Leung A C, Lau W Y S, Tranter A D, Paul K V, Rambach M, Buchler B C, Lam P K, White A G and Weinhold T J 2024 *APL Quantum* **1** 036102
[14] Duranti S, Wengerowsky S, Feldmann L, Seri A, Casabone B and de Riedmatten H 2024 *Opt. Express* **32** 26884
[15] Zhou Z-Q, Lin W-B, Yang M, Li C-F and Guo G-C 2012 *Phys. Rev. Lett.* **108** 190505
[16] Wei S-H *et al* 2024 *npj Quantum Inf.* **10** 19
[17] Businger M, Nicolas L, Mejia T S, Ferrier A, Goldner P and Afzelius M 2022 *Nat. Commun.* **13** 6438
[18] Bonarota M, Le Gouët J-L and Chanelière T 2011 *New J. Phys.* **13** 013013
[19] Zhang S, Shi J, Cui Z, Wang Y, Wu Y, Duan L and Pu Y 2024 *Phys. Rev.* X **14** 21018
[20] Chang W, Li C, Wu Y-K, Jiang N, Zhang S, Pu Y-F, Chang X-Y and Duan L-M 2019 *Phys. Rev.* X **9** 041033
[21] Körber M, Morin O, Langenfeld S, Neuzner A, Ritter S and Rempe G 2018 *Nat. Photon.* **12** 18
[22] Ortu A, Holzäpfel A, Etesse J and Afzelius M 2022 *npj Quantum Inf.* **8** 29
[23] Collins O A, Jenkins S D, Kuzmich A and Kennedy T A B 2007 *Phys. Rev. Lett.* **98** 060502
[24] Sangouard N, Simon C, de Riedmatten H and Gisin N 2011 *Rev. Mod. Phys.* **83** 33
[25] Zhao B, Chen Y-A, Bao X-H, Strassel T, Chuu C-S, Jin X-M, Schmiedmayer J, Yuan Z-S, Chen S and Pan J-W 2009 *Nat. Phys.* **5** 95
[26] Heshami K, England D G, Humphreys P C, Bustard P J, Acosta V M, Nunn J and Sussman B J 2016 *J. Mod. Opt.* **63** 2005
[27] Ma Y, Ma Y-Z, Zhou Z-Q, Li C-F and Guo G-C 2021 *Nat. Commun.* **12** 2381
[28] Heinze G, Hubrich C and Halfmann T 2013 *Phys. Rev. Lett.* **111** 033601
[29] Schraft D, Hain M, Lorenz N and Halfmann T 2016 *Phys. Rev. Lett.* **116** 073602
[30] Guo M, Liu S, Sun W, Ren M, Wang F and Zhong M 2023 *Front. Phys.* **18** 21303
[31] Nunn J, Reim K, Lee K C, Lorenz V O, Sussman B J, Walmsley I A and Jaksch D 2008 *Phys. Rev. Lett.* **101** 260502
[32] de Riedmatten H, Afzelius M, Staudt M U, Simon C and Gisin N 2008 *Nature* **456** 773
[33] Afzelius M, Simon C, de Riedmatten H and Gisin N 2009 *Phys. Rev.* A **79** 052329
[34] Ortu A, Rakonjac J V, Holzäpfel A, Seri A, Grandi S, Mazzera M, de Riedmatten H and Afzelius M 2022 *Quantum Sci. Technol.* **7** 035024
[35] Fleischhauer M, Imamoglu A and Marangos J P 2005 *Rev. Mod. Phys.* **77** 633
[36] Gorshkov A V, André A, Lukin M D and Sørensen A S 2007 *Phys. Rev.* A **76** 033805

[37] Fraval E, Sellars M J and Longdell J J 2005 *Phys. Rev. Lett.* **95** 030506
[38] Fraval E, Sellars M J and Longdell J J 2004 *Phys. Rev. Lett.* **92** 077601
[39] Longdell J J, Alexander A L and Sellars M J 2006 *Phys. Rev.* B **74** 195101
[40] Nilsson M, Rippe L, Ohlsson N, Christiansson T and Kröll S 2002 *Phys. Scr.* **T102** 178
[41] Nilsson M, Rippe L, Kröll S, Klieber R and Suter D 2004 *Phys. Rev.* B **70** 214116
[42] Lauritzen B, Timoney N, Gisin N, Afzelius M, de Riedmatten H, Sun Y, Macfarlane R M and Cone R L 2012 *Phys. Rev.* B **85** 115111
[43] Hain M, Stabel M and Halfmann T 2022 *New J. Phys.* **24** 023012
[44] Chang T, Tian M, Mohan R K, Renner C, Merkel K D and Babbitt W R 2005 *Opt. Lett.* **30** 1129
[45] Kozhekin A E, Mølmer K and Polzik E 2000 *Phys. Rev.* A **62** 033809
[46] Equall R W, Cone R L and Macfarlane R M 1995 *Phys. Rev.* B **52** 3963
[47] Graf F R, Renn A, Zumofen G and Wild U P 1998 *Phys. Rev.* B **58** 5462
[48] Gorshkov A V, André A, Fleischhauer M, Sørensen A S and Lukin M D 2007 *Phys. Rev. Lett.* **98** 123601
[49] Novikova I, Gorshkov A V, Phillips D F, Sørensen A S, Lukin M D and Walsworth R L 2007 *Phys. Rev. Lett.* **98** 243602
[50] Holzäpfel A 2022 *PhD Dissertation* Univ. Geneva
[51] Viola L, Knill E and Lloyd S 1999 *Phys. Rev. Lett.* **82** 2417
[52] Genov G T, Schraft D, Vitanov N V and Halfmann T 2017 *Phys. Rev. Lett.* **118** 133202
[53] Carr H Y and Purcell E M 1954 *Phys. Rev.* **94** 630
[54] Meiboom S and Gill D 1958 *Rev. Sci. Instrum.* **29** 688
[55] Genov G T, Schraft D and Halfmann T 2018 *Phys. Rev.* A **98** 063836
[56] Zambrini Cruzeiro E, Fröwis F, Timoney N and Afzelius M 2016 *J. Mod. Opt.* **63** 2101
[57] Xu Z, Wu Y, Tian L, Chen L, Zhang Z, Yan Z, Li S, Wang H, Xie C and Peng K 2013 *Phys. Rev. Lett.* **111** 240503